*Proceedings of the Second International Conference on Press-in Engineering 2021, Kochi, Japan – Matsumoto et al (eds)*


# A centrifuge model study on laterally loaded large diameter steel tubular piles socketed in soft rock

V. Kunasegaram
*South Eastern University of Sri Lanka, Oluvil, Sri Lanka*

J. Takemura
*Tokyo Institute of Technology, Tokyo, Japan*

Y. Ishihama
*Nippon Steel and Sumitomo metal Corporation, Chiba, Japan*

Y. Ishihara
*GIKEN LTD, Tokyo, Japan*

ABSTRACT: This paper discusses the influence of rock socket depths on the deformation and failure mechanism of rock socketed piles under a constant vertical eccentricity of 6.5 m. For the centrifuge model study, two types of model soft rock ground were prepared, a single soft rock layer and a soft rock layer with overlying sand. Lateral resistance of piles with three different rock socket depths were investigated in both model grounds at 50g centrifugal acceleration. From the loading tests, two different failure modes were observed, i.e., ground failure and pile structural failure depending on the embedment depth and the ground conditions. For the piles with relatively small socket depth ($d_R$) in a single rock layer, the increase of $d_R$ can increase the lateral and moment resistance. However, as the $d_R$ increases, the effect of $d_R$ becomes less significant, especially for ultimate resistance due to the pile structural failure.

## 1 INTRODUCTION

Thanks to the high structural stiffness of large diameter piles and the development of novel installation technique, recently the application of large diameter steel tubular piles in hard ground, such as soft to medium-hard rock has increased in engineering projects around the world (IPA). Large diameter steel pipe piles can be applied for various large geotechnical structures, such as the mono-pile foundation for offshore wind turbine and large height cantilever type retaining wall. Lateral response of mono-pile foundations in sand was quite deeply investigated through 1g laboratory tests and more sophisticated centrifuge models by several researchers. However, as described in Lehane and Guo (2017), the documented literature to illustrate the mechanical behaviour of rock socketed large-diameter steel tubular piles under lateral loading is extremely rare. Perhaps it could be attributed to the difficulties of conducting large scale tests in a hard medium to observe the critical behaviour, which is controlled by several influential factors, such as pile factors (diameter, stiffness), ground factors (strength and stiffness), and loading factors (loading height, monotonic and cyclic). On the other hand, a few field tests have been conducted on concrete shafts and some centrifuge tests were also conducted for modelling caisson and solid piles in various types of rock as summarized in Kunasegaram and Takemura,(2020). In most of the previous field and physical model studies, the points of loading were almost closer to the ground surface except the field tests done by Digioia and Rojas- Gonzalez (1994). These loading conditions are different from the abovementioned target structures. A typical loading condition for both, the mono-pile foundation and the large height self-standing wall is a relatively large moment load due to one-way cyclic lateral loads induced by wind loads and seismic excitations, respectively. Therefore, as a preliminary study, authors have conducted few single pile lateral loading tests with a constant vertical eccentricity of 6.5 m at 50g centrifugal acceleration to understand the deformation and failure mechanism of rock socketed single piles. This paper reports the influences of rock socket depth on the deformation and failure mode of single piles embedded in stiff grounds. Also it describes the loading history on the behavior of single piles.

DOI: 10.1201/9781003215226-31

## 2 CENTRIFUGE MODELLING

### 2.1 *Centrifuge models and test procedures*

Two different ground conditions were made in the centrifuge models, namely soft sand rock and soft rock overlaid by the medium dense Toyoura sand (Dr =80%). Centrifuge model arrangement for the piles embedded in above grounds are shown in Figures 1(a) and 1(b) respectively. A container with the internal dimensions of 700 mm length, 500 mm depth and 150 mm width was used in both models. Model tubular piles used in this study were thin wall pipes with 40 mm outer diameter and 0.5 mm thickness, made of stainless steel (SUS304) having the young's modulus ($E$) of 193 GPa and yield stress ($\sigma_y$) of 255 MPa. At the pile top, a solid circular pile cap made of aluminum with 30mm socketed depth was tightly fixed to form a solid loading head (Figure 1(c)). Sectional and mechanical properties of steel tubular piles are described together with the other test conditions in Table.1. Detailed mechanical properties of Toyoura sand were reported by Tatsuoka et al, (1986) including the effects of density, and the mechanical properties of model soft rock used was described in Kunasegaram and Takemura, (2020). The model piles were equipped with bending strain gauges on both sides of the pile along the loading direction, and Wheatstone circuits were made with the help of bridge boxes. Bending strains were measured by using full bridge circuits along the pile, while at the pile tip a pair of half bridge circuits were utilized to measure the axial strains at the loading and the opposite sides independently. Centrifuge model arrangement for three single piles embedded ($d_e$=40 mm, Pile-S; 60 mm, Pile-M; 80 mm, Pile-L) in soft sand rock (Model-4) is described in Figure 1 (a). In the preparation of soft rock model, 300 mm thick acrylic plates stack was tightly placed in the container bottom to reduce the depth to 200 mm. A 190 mm thick layer of soft sand rock was made by compacting sand-clay-cement mixture layer by layer with 30 mm thickness, confirming the target unit weight of each layer of compacted mixture. Immediately after casting the mixture, the model tubular piles were installed vertically into the unsolidified mixture with a pile guide to the specified depth, and fixed the pile position. The casted mixture was cured for 14 days in order to achieve the targeted strength ($q_u$) and stiffness of the embedded medium. The detailed preparation procedures and mechanical properties of the soft sand rock material are reported by Kunasegaram et al, (2015). It is important to note that sand and soft rock was filled inside the pile up to the rock surface level with the pile installation process employed in the model preparation stage, which was confirmed by means of physical measurements. In the preparation of Model-5 with two-layers ground (Figure 1(b)), 160 mm thick acrylic plates stack was placed at the container bottom to make 340 mm depth for the sample. Then a 200 mm thick soft rock layer was made and the model piles were installed in the soft rock layer with the rock socked depths ($d_R$) same as the $d_e$ of Model-4. After 14 days curing for the soft rock, a 130 mm thick top sand layer with Dr=80% was made by air pluviation. It must be emphasized that the pile SP_SR_2* in Model-4 was accidently preloaded about 1 mm prior to the test without instrumentation and the stiffness and resistance could not be obtained in the intact condition for the small displacement range. Therefore, to study the behavior of pile with short socket ($d_e$=2 m) and to confirm the repeatability, three single piles were tested in Model-8 with the identical embedment depths of model-4 and slightly different imposed displacement cycles as described in Table- 2.

Upon completion of the model, the loading jack and laser displacement sensors (LDTs) were mounted on the container. Thereon the container moved to centrifuge platform and rigidly fixed, then the centrifugal acceleration was increased up to 50g. One-way horizontal load cycles were applied by the jack from small to large pile top displacements as described in Figure 2 at 50g environment. Applied horizontal load at the pile top ($P_L$) was measured by a load cell and horizontal

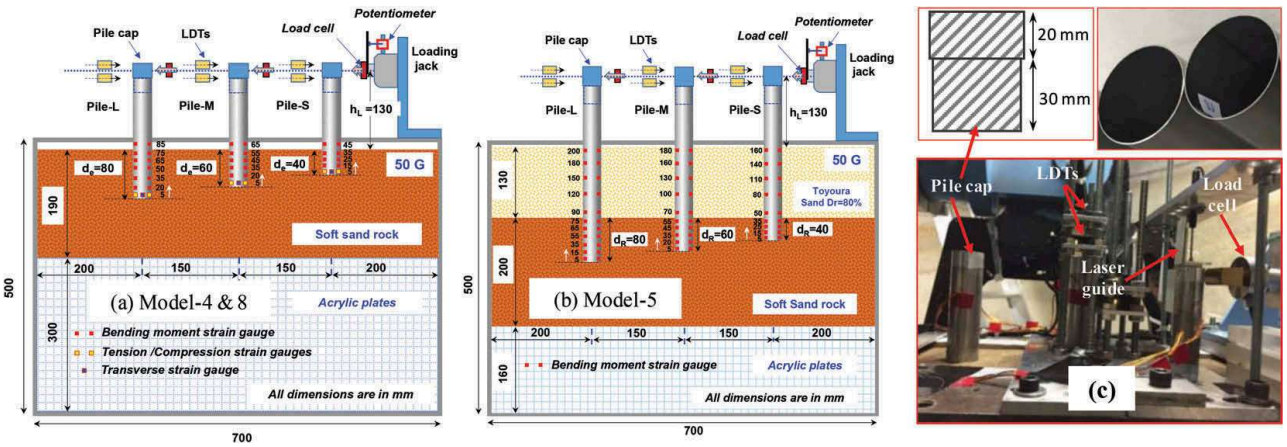


Figure 1. Centrifuge model arrangements.

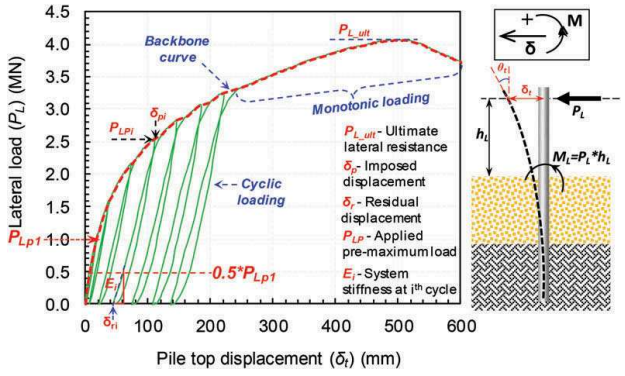


Figure 2. One way cyclic loading and sign conventions defined in the loading sequence.

displacement ($\delta_t$) and rotation ($\theta_t$) at the pile top was obtained by means of LDTs at two elevations as described in Figure 1(a,b). Having completed one loading test, the centrifuge was once stopped and the loaded pile was removed. Resetting the jack and LDTs to the next pile and the same horizontal loading was repeated. The loading was conducted in the sequence of Pile-S, Pile-M and Pile-L. In the following chapter, the test results are shown in prototype scales.

## 3 RESULTS AND DISCUSSION

### 3.1 *Observed load-displacement behaviours*

A typical cyclic load ($P_L$) –displacement ($\delta_t$) behaviours for the piles embedded in SR (SP_SR_4) and MS_SR ground (SP_MS_SR_4) are drawn in Figure 3(a). The Figure 3(a) describes the imposed displacement cycles with increasing mean load and cyclic displacement amplitudes. Corresponding moment load (at the ground level, $M_L = P_L * h_L$) - pile top rotation ($M_L$-$\theta_t$) relation for the piles is also illustrated in Figure 3(b). The imposed pre-maximum displacements ($\delta_{Pi}$) and applied pre-maximum loads ($P_{LPi}$) in each cycle are summarised in Table 2 for all the piles given in Table 1. The loading sequence in this study consists of a limited number of one-way load cycles and a subsequent monotonic loading up to the ultimate failure of the system, determined by either the failure of embedment ground or structural buckling.

In each unloading-reloading cycle, a certain amount of residual displacements can be seen (Figure 3(a)) after the unloading, which pinpoints the plastic deformations of the embedded medium even at relatively small $\delta_{Pi}$'s. Although this residual displacement ($\delta_{ri}$) is eventually accumulated in each cycle, the $P_L$- $\delta_t$ relation in reloading processes returns to a unique curve, which is the envelope (Figure 2) of cyclic load-displacement behaviour. Here onwards the envelope curve will be written as the backbone curve.

Figure 4(a) and Figure 4(b) show the backbone curves of $P_L$- $\delta_t$ and $M_L$- $\theta_t$ relationships obtained in the loading sequences of all the piles, respectively.

The influence of embedded medium and embedment depth ($d_e$) on the lateral and rotational resistances of large diameter piles under identical loading conditions can be confirmed from Figure 4(a) and Figure 4(b), respectively. From Figure 4(a), the deeper the rock socketing is, the larger the mobilized resistance of pile can be observed in the overall load displacement behaviour. However, based on Figure 4 (a) and Figure 4(b), there is no significant difference in the lateral and rotational resistances between the two piles Model-5 (SP_MS_SR_3, SP_MS_SR_4). This observation implies the insignificance in the increment of socketing over 3 m (1.5Φ) in the underlain rock strata for the case of MS_SR ground. Although increasing the socketing depth from 3 m to 4 m has no significant influence on the lateral resistance of socketed piles in the two-layer profile, the comparison between SP_MS_6.5 and SP_MS_SR_2

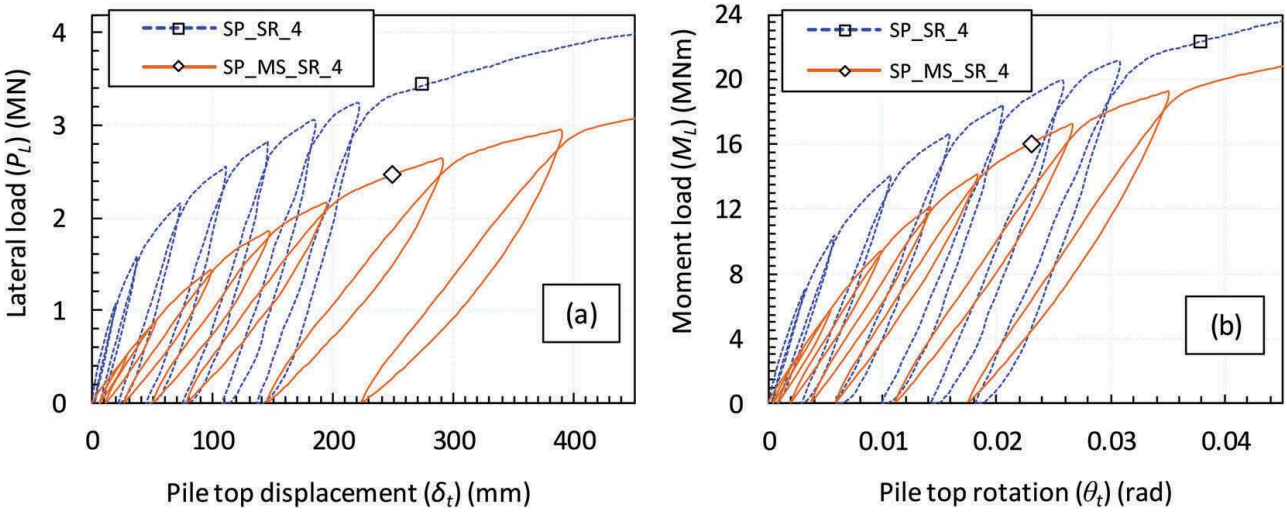


Figure 3. Typical (a) cyclic load – displacement and (b) moment load- rotation behaviour observed at pile top for the piles in single rock layer (SP_SR_4) and two layer (SP_MS_SR_4) profile.

Table 1. Model conditions and properties of embedment medium.

| Model condition | Properties of embedment medium | Pile notation | Embedment depth ($d_e$) | $E_e/G^*$ | Pile properties *EI*, $M_y$, $M_p$ |
|---|---|---|---|---|---|
| **Model-4** Soft rock (SR) | $\gamma_{tr}$ =20.1 kN/m$^3$ | SP_SR_2* | 2 m [40 mm] | 60 | Φ=2 m (40 mm) |
| | $\gamma_{dr}$=16.8 kN/m$^3$ | SP_SR_3 | 3 m [60 mm] | 60 | |
| | $q_u$ =1.4 Mpa | | | | |
| | $E_r$ =660 Mpa | SP_SR_4 | 4 m [80 mm] | 60 | |
| **Model-5** Soft rock (SR) overlain by Toyoura sand (MS) Dr=80% | $\gamma_{tr}$ =20.1 kN/m$^3$ | SP_MS_SR_2 | $d_s$=6.5 m [130 mm] | | t = 25 mm (0.5 mm) |
| | $\gamma_{dr}$=16.8 kN/m$^3$ | | $d_R$=2m [40 mm] | | |
| | $q_u$ =1.4 Mpa | SP_MS_SR_3 | $d_s$=6.5 m [130 mm] | | |
| | $E_r$ =660 Mpa | | $d_R$=3m [60 mm] | | *EI*=14.6 GNm$^2$ (2.34 kNm$^2$) |
| | $\gamma_{ds}$=15.5 kN/m3 | SP_MS_SR_4 | $d_s$=6.5 m [130 mm] | | |
| | $\phi' = 41°$ | | $d_R$=4m [80 mm] | | |
| **Model-8** Soft rock (SR) | $\gamma_{dr}$=16.8 kN/m3 | SP_SR_2× | 2 m [40 mm] | 60 | $M_y$=19.3 MNm (154 Nm) |
| | $q_u$=1.4 Mpa | SP_SR_3× | 3 m [40 mm] | 60 | $M_p$=24.8 MNm |
| | $E_r$=660 MPa | SP_SR_4× | 4 m [40 mm] | 60 | (198 Nm) |

* Preloaded prior to the test without instrumentation
$d_s$=Embedment depth in sand layer
$d_R$=Socketing depth in rock
Loading height, $h_L$= 6.5 m for all the piles
$M_y$: Theoretical yielding bending moment of the pile
$M_p$: Theoretical bending moment causing the plastic failure of pile
All dimensions are given in prototype scale, model scales are given in brackets

Table 2. Imposed pre-maximum displacements and pre-maximum loads applied in each cycle.

| | Imposed pre-maximum displacement ($\delta_{Pi}$ in %$\phi$)/Pre-maximum load (*PLPi* inMN) in each one way loading cycles, N = cycle number | | | | | | | |
|---|---|---|---|---|---|---|---|---|
| Pile notation | N=1 | N=2 | N=3 | N=4 | N=5 | N=6 | N=7 | N=8 |
| SP_SR_2* | 2.3/0.56 | 4.1/0.78 | 5.8/0.90 | 7.7/0.98 | 9.6/1.06 | - | - | - |
| SP_SR_3 | 0.8/0.84 | 1.8/1.24 | 3.7/1.54 | 5.6/1.74 | 7.6/1.90 | 9.4/2.02 | - | - |
| SP_SR_4 | 1.0/1.08 | 1.9/1.58 | 3.7/2.14 | 5.6/2.56 | 7.3/2.82 | 9.3/3.08 | 11.1/3.26 | - |
| SP_MS_SR_2 | 1.3/0.48 | 2.4/0.78 | 4.9/1.14 | 7.4/1.40 | 9.9/1.62 | 14.7/2.00 | 19.6/2.34 | - |
| SP_MS_SR_3 | 1.1/0.44 | 2.4/0.82 | 4.7/1.32 | 7.2/1.66 | 9.8/1.98 | 14.3/2.40 | 19.4/2.78 | - |
| SP_MS_SR_4 | 1.4/0.52 | 2.7/0.88 | 5.0/1.42 | 7.4/1.86 | 9.8/2.18 | 14.6/2.66 | 19.5/2.96 | - |
| SP_SR_2× | 1.5/0.58 | 2.6/0.72 | 4.9/0.84 | 7.4/0.92 | 10.3/0.96 | 13.2/0.96 | 16.0/0.96 | 19.1/1.00 |
| SP_SR_3× | 1.1/1.14 | 2.3/1.44 | 4.7/1.78 | 7.1/1.98 | 9.3/2.14 | 11.6/2.28 | 13.9/2.40 | 16.3/2.48 |
| SP_SR_4× | 1.1/1.04 | 2.4/1.48 | 4.6/2.00 | 6.9/2.40 | 9.2/2.66 | 11.7/2.92 | 14.4/3.14 | 16.7/3.28 |

* Preloaded prior to the test without instrumentation
Imposed displacements and Pre-maximum loads are given in prototype scale

indicates the significant contribution of 2 m socketing into relatively hard layers. Lateral resistance of pile SP_MS_SR_2 increased more than twice in the overall response than that of the non-socketed pile SP_MS_6.5. Structural failures of the pile were confirmed with clear local buckling at a point below the ground level as shown in Figure 5(b) for all three socketed piles in the two-layer profile.

However, the buckling point of SP_SR_4 is located at the ground surface level which could be attributed to the large lateral confinement of soft rocks and the plugged portion of the rock inside the piles. Once the pile failed by the structural buckling, the further increase of socketing depth ($d_R$ >3 m for socketed piles) could have no significant influence on the lateral resistance of piles for the abovementioned loading conditions. The reductions of resistance in Figure 4(a) after the peak load for the piles in MS_SR ground are the indication of clear structural failure, while for non-socketed pile SP_MS_6.5, the resistance increased until large pile top displacement over 50% of pile diameter ($\Phi$)

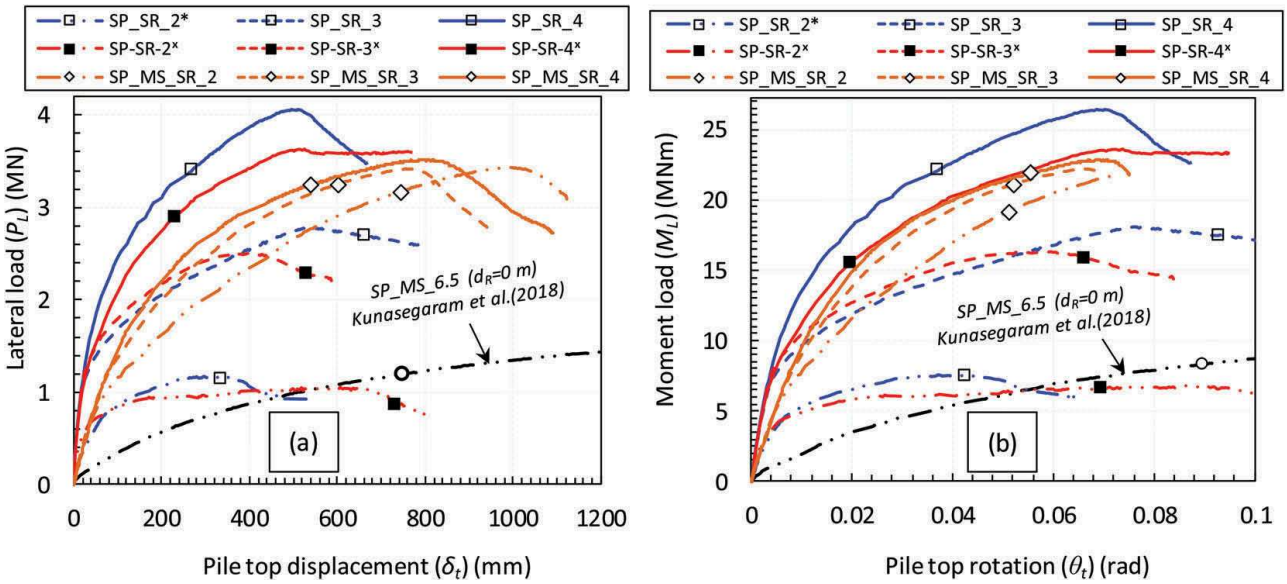


Figure 4. Backbone curves of (a) Lateral load - pile top displacement and (b) moment load-pile top rotation.

without showing peak resistance also no structural failure can be observed from Figure 4(a). For the piles embedded in the soft sand rock, 1 m increment in embedment depth can significantly increase the ultimate lateral resistance up to $d_e$=4 m. As a clear structural failure with local buckling was observed slightly above the ground level for SP_SR_4 with $d_e$=4m as shown in Figure 5(a), it can be inferred that further increase of the embedment could not provide substantial contribution to the pile lateral resistance. The depth over which the effect of embedment increment cannot be obtained is considered as an "optimum embedment depth (OED)". The difference of OED in the soft rock and socketed piles can be attributed to their rigidity or confinement. However, the pile with identical embedment (SP_SR_4ˣ) in Model-8 exhibited the rock splitting as the ultimate failure mode, and no visible local deformations appeared in the pile (Figure 5(a)). The different failure mechanisms of piles with identical $d_e$ could be attributed to two reasons as follows.

The $d_e$ =4 m is closer to the critical $d_e$ for the implemented loading condition, around this $d_e$ the failure mode can be easily alternated from the ground failure to the pile structural failure and vice versa, by loading cycles or loading sequence. The other reason is the difference in the imposed pre-maximum displacement ($\delta_{Pi}$) sequence of two piles, where the pile SP_SR_4ˣ experienced larger $\delta_{Pi}$'s compared to SP_SR_4 in each cycle (see Table 2). Besides the ultimate failure mechanism of these two piles, smaller mobilised resistance of pile SP_SR_4ˣ than the pile SP_SR_4 at small $\delta_{Pi}$'s ($\delta_t$ =2%Φ (40mm)) could be resulted by unforeseen irregularities of rock in the toe back regime. It can be confirmed from normalized deflection profiles discussed in the subsequent chapter, where the bottom tip displacements of pile SP_SR_4ˣ is higher from the early stage of loading. Furthermore, structural failures were not observed for the piles SP_SR_2*, SP_SR_2ˣ, SP_SR_3 and SP_SR_3ˣ, but the load displacement curves of these piles also showed a peak resistance and subsequent reduction. These behavior of the piles with no pile failure but ground failure of the soft rock is different from that of the pile (SP_MS_6.5) in sand. This can be attributed to the strain softening of stress-strain relationship of the rock material and smaller $d_e$ of the soft rock model than that of sand model. Although the piles with structural failure and the piles embedded in the soft rock with relatively small embedment depth (SP_SR_2*, SP_SR_2ˣ, SP_SR_3 and SP_SR_3ˣ) also showed strain softening behavior in the load displacement curves, the post peak resistance reduction are different between the piles failed by the structural failure and the ground failure. Once the structural buckling initiated a sudden reduction of load against the displacements can be seen. On the other hand, the observed post peak behavior related to ground failures exhibited smaller post peak stiffness and much more ductile especially for the deeper embedment condition (SP_SR_3 and SP_SR_3ˣ)).

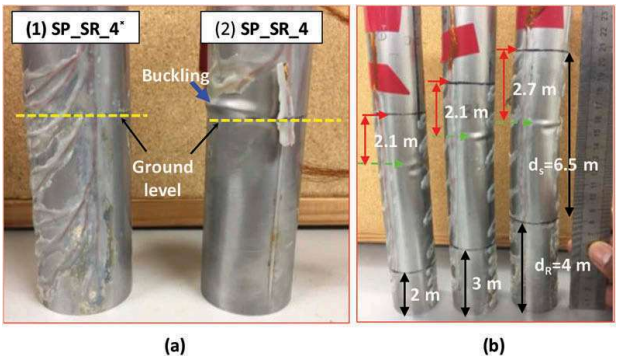


Figure 5. Observed structural deformation of piles in (a) single rock layer and (b) two layer profile.

### 3.2 *Influence of embedment depth*

The influence of embedment ($d_e$) or socketing depth ($d_R$) on lateral resistance of rock socketed piles from small to large pile top displacements ($\delta_t$) are depicted in Figure 6. It is important to note that the load corresponding to the pile top displacements of $\delta_t$ =40% Φ was considered as ultimate resistance ($P_{L\_ult}$) for the pile (SP_MS_6.5) without peak resistance in the load - displacement relation. From Figure 6, a distinctive behavior of piles at different displacement levels depending on the stiffness of embedded medium can be observed. The horizontal resistance of piles socketed in SR ground ($d_e$=$d_R$) (Model-4 & 8) increased with $d_e$, but the trend is highly influenced by the imposed displacement. In Model-4 and 8, significantly large increase of lateral resistance can be attained by a small increment (0.5Φ and1Φ) of $d_e$ from 2 m to 4 m, exhibiting the large lateral confinement of rock type materials even with small socketing (Φ to 2Φ) depths. The variation of lateral resistance is almost linearly increasing with $d_e$ for all displacements, except the piles with $d_e$ over 3 m at small displacements. Lateral resistance of the pile with $d_e$=3 m (SP_SR_3, SP_SR_3$^x$) is almost the same as $d_e$ = 4 m (SP_SR_4, SP_SR_4$^x$) at $\delta_t$ = 0.5%Φ and 1%Φ in Model- 4, similar behaviour can be seen up to $\delta_t$ = 2%Φ in Model-8. The distinctive behaviour at these small imposed displacements could be attributed to the lateral confinement given by shallower depth of the rock (less than 3m) at their intact condition. As the loading progresses beyond $\delta_t$ =1%Φ, the softening of rock by the increase of displacement deteriorates the subgrade reaction of shallow rock layers and cause the difference in resistance between the piles with $d_e$ = 3 m and $d_e$ = 4 m. Although the pile with $d_e$ = 4 m in Model -8 exhibits smaller resistance compared to that of Model-4 from $\delta_t$ =2%Φ to $P_{L\_ult}$, the increasing tendency is similar in both models. Furthermore, the smaller ultimate resistances of all three piles in Model-8 could be attributed to the cyclic weakening mechanism due to relatively large imposed displacements (Table-2) than that of Model-4. Influence of socketing depth ($d_R$) on the lateral resistance of piles embedded in MS_SR ground also could be explained from Figure 6. Comparing the piles with $d_R$ = 0 (SP_MS_6.5) and $d_R$ = 2 m (SP_MS_SR_2), the lateral resistance of piles can be increased about three times from the early stage of loading to the ultimate condition, by a $d_R$ of Φ into the underlain soft rock layer. In Model-5, the influence of $d_e$ ($d_e$=$d_s$+$d_R$) is differently appeared in the mobilised resistance depending on the imposed $\delta_t$. From Figure 6, $d_R$ over 2 m has no significant influence on the lateral resistance up to $\delta_t$ = 2%Φ. However, a clear influence of $d_R$ tends to appear from $\delta_t$ = 4%Φ to 10%Φ and again the influence of $d_R$ over 2 m becomes insignificant on the $P_{L\_ult}$ of piles in MS_SR ground as seen in Figure 6. From the variation of ultimate resistances against $d_e$ in Figure 6 and observed failures (Figure 5) of rock socketed piles in Model-4,5 and 8 it can be confirmed that, if the pile structural failure determines the ultimate failure condition the effect of $d_R$ becomes insignificant, contrarily ultimate resistances of ground failure conditions are highly influenced by $d_R$. As overall behaviour, it can be concluded that the lateral resistance of pile embedded in sand and soft rock increases with increasing $d_e$ if the ground stiffness determines the ultimate resistance. However, the effect of the embedment over the optimum depth has no significant contribution. On the other hand, due to the softening of ground materials and the change of failure mode from the ground failure to pile structural failure, the optimum embedment depth changes depending on the conditions of resistance, which is shallower for the initial stiffness than the ultimate loading conditions in the soft rock.

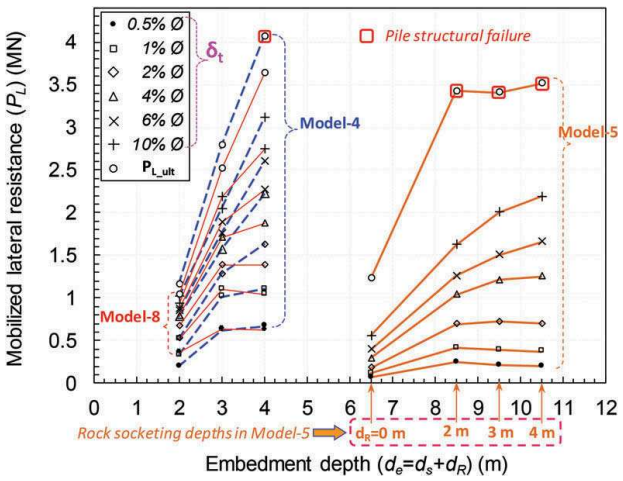


Figure 6. Influence of rock socketing depth on the lateral resistances of the piles single rock layer and two layer profile.

### 3.3 *Measured nominal bending moments*

Measured bending moments along the pile at different pile top displacements (0.1%, 0.5%, 1%, 2%, 4% & 10% Φ) for the piles in all three centrifuge models are presented in Figure 7. From Figure 7(a) to 7(f), the bending moments of the pile in the overlain sand layer increase almost linearly with the distance from the loading point to the depth of -2 m. The observation clearly indicates that the confining stresses from shallow layers (up to Φ) of sand has less significant influence on the lateral resistance of piles. On the other hand, the piles in the soft rock showing the maximum moment slightly above the ground surface and an abrupt change in the bending moments above and below the ground surface also can be observed. This observed bending behavior is another evidence of very high confinement of shallow layers of soft rock. A high degree of radial and circumferential restraint could be expected closer to the rock surface due to the high confinement of rock type materials. It results in higher circumferential membrane stresses

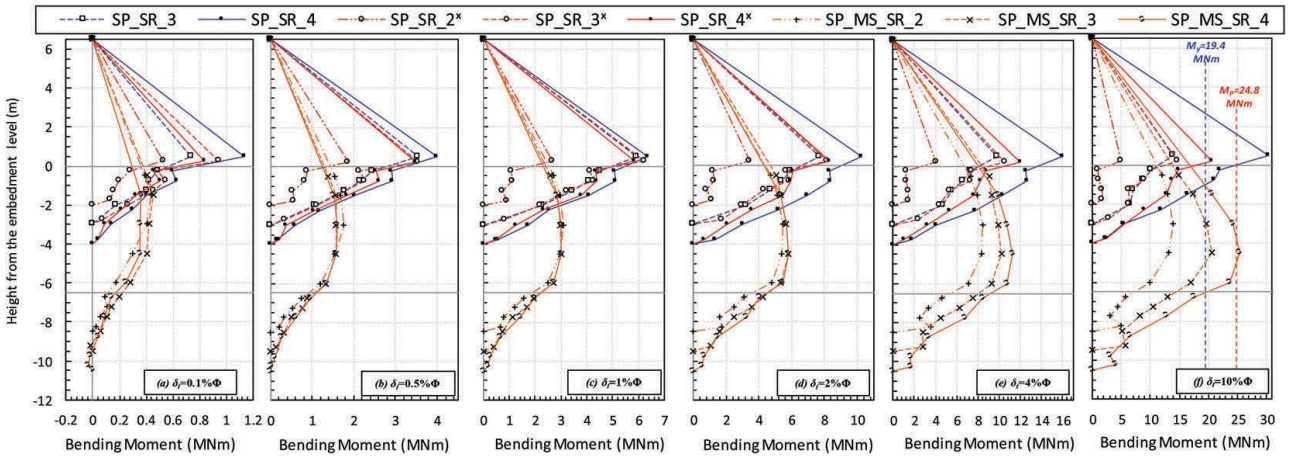


Figure 7. Observed bending profiles at different Imposed displacement amplitudes.

in a pile, and the influence of membrane action could be expected up to a distance of Φ above the rock surface, as described in Kunasegaram and Takemura (2021). As a consequence of membrane stresses, the measured nominal bending strains become larger than that of real bending strains which corresponds to a pure bending behaviour of the pile. Therefore, the observed abrupt changes could be resulted by stress discontinuity at the embedment level and a certain degree of local deformations of tubular pile.

From Figure 7, at small imposed displacements ($\delta_t$ <2%Φ), the difference between the bending moments of piles with different $d_R$ in MS_SR ground is insignificant. However, as the displacement increases, pile with larger $d_R$ shows the larger bending moment. Also, the depths of maximum bending moment in the sand layer of MS_SR ground are deeper for the pile with large $d_R$ than small $d_R$. The observation implies that the effect of the deterioration of soft rock stiffness at the shallow layers affected the lateral resistance over $\delta_t$=2%Φ, it can be confirmed from the variation of lateral resistance illustrated in Figure 6 for the piles in Model-5. Up to the displacement, $\delta_t$=4%Φ ($\delta_t$=80 mm) the bending moments of all the piles are smaller than the yielding moment ($M_y$). At $\delta_t$ =10%Φ ($\delta_t$=200 mm), SP_SR_4, SP_SR_4$^x$, SP_ MS_SR_3 & SP_ MS_SR_4 exhibit the bending moments more than $M_y$. In which, the bending moment of SP_SR_4 and SP_MS_SR_4 became more than that of the plastic hinge ($M_p$). It should be noted that the moments over $M_y$ are not actual mobilized moments in a pile, but they are the nominal ones calculated from the strain measurement. None the less, these results well agree with the structural deformations observed in Figure 5.

### 3.4 *Deformation modes and failure mechanism*

As described in Figure 8(a), the PT displacement ($\delta_t$) can be divided into three components; (a) displacement at the RS ($\delta_{RS}$), (b) displacement caused by the rotation at RS ($h_L$*$\theta_{RS}$) and (c) displacement caused by the bending of pile above the RS ($\delta_{t\_b}$). These three components are considered as indices representing the effects of translation, rotation, and bending of a laterally loaded pile in SR ground, respectively. Similarly, the three components of PT and SS displacements for the piles in MS_SR ground are defined in Figure 8(b) in terms of displacements and rotations at SS and RS levels. The corresponding variation of displacements and rotations against the moment load for the piles in SR (Figure 8(c), (d)) and MS_SR grounds (Figure 8(e), (f)) are illustrated in Figure 8. From Figure 8(c,d), relatively small displacements and rotations at RS level with a linearly increasing trend prior to the yielding deformations and subsequent progression of a nonlinear variation against the $M_L$ could be observed as a typical behaviour of piles in SR ground. However, the piles in MS_SR ground exhibits relatively large displacement and rotations at SS with a nonlinear variation even at small $M_L$ (Figure 8(e,f)). Mechanism behind these distinctive behavior of piles in SR and MS_SR ground can be explained using Figure 9. The percent fractions of $\delta_t$ representing the effects of translation, rotation and bending against the $\delta_t/\Phi$ for the piles in both SR and MS_SR grounds are described in Figure 9. Comparing Figure 9(a) and Figure 9(b) the translational fraction ($\delta_{RS}$) of piles in SR ground are less than 10% at the beginning and much smaller compared to bending and rotational fractions even at large $\delta_t/\Phi$. Thanks to the higher initial stiffness of intact rock sockets, which effectively hold the pile prior to the rock yielding. However, the translational fraction ($\delta_{GS}$) of piles in MS_SR ground governs more than 30% of $\delta_t$ from the beginning of loading. The above observation could be attributed to relatively small subgrade modulus of overlain sand compared to SR and the higher fixity of rock sockets, which allows significant bending of the pile in the sand layer. It can be confirmed from the bending fraction representing the SS displacements as illustrated in Figure 9(c) and the bending profiles in Figure 10.

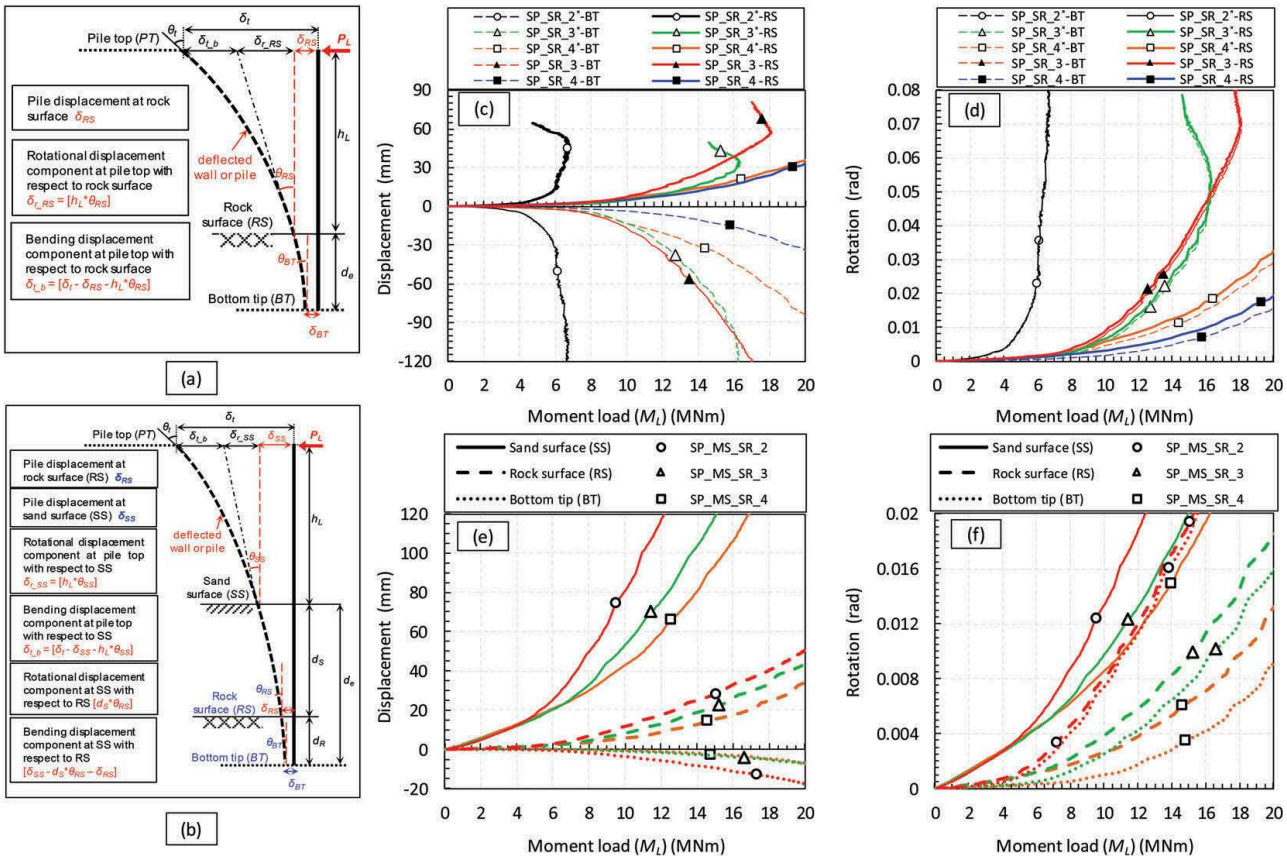


Figure 8. (a,b) Typical deflection profiles and the variation of (c,e) displacements and (e,f) rotations at sand surface, rock surface and bottom tip against the applied moment load ($M_L$=$P_L$*$h_L$) for the rock socketed piles.

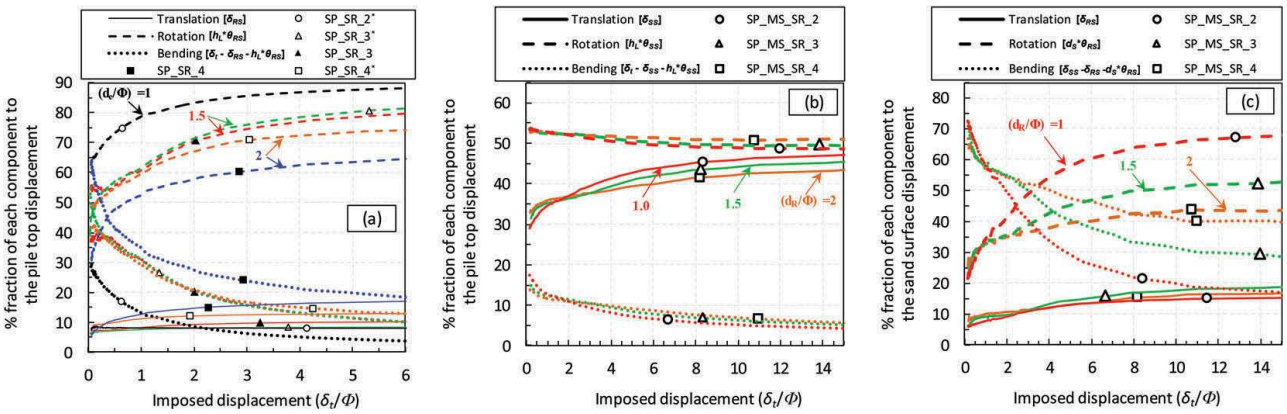


Figure 9. Variation of % fraction displacement components of (a,b) pile top (PT) displacement and (c) sand surface (SS) displacement against the normalized imposed displacements for rock socketed piles.

Deformation modes of rock socketed piles in a single rock layer, and the mode change with the increase of moment load and imposed displacements could be explained from Figure 8(c,d), Figure 9(a) and the variation of normalized deflection profiles illustrated at different $\delta_t/\Phi$ values in Figure 10. From Figure 8(c,d), Figure 9(a) the pile SP_SR_2× with a short socket depth ($d_R/\Phi$ = 1.0) exhibits a vertical increase of RS, BT displacements and rotations beyond a moment load of 6 MNm. Furthermore, identical rotations at RS($\theta_{RS}$), BT($\theta_{BT}$) in Figure 8(d) and a larger rotational fraction (about 65%) from the initiation loading with a continuously increasing and decreasing trends of both rotational ($h_L*\theta_{RS}$) and bending ($\delta_t$ - $\delta_{RS}$ -$h_L*\theta_{RS}$) fractions against $\delta_t/\Phi$ (Figure 9(a)) clearly dictate a brittle failure with an activated rotational mode. The above failure took place due to the extension of toe- back shear deformations (Kunasegaram and Takemura (2021)) with a pivot point of pile SP_SR_2× located around

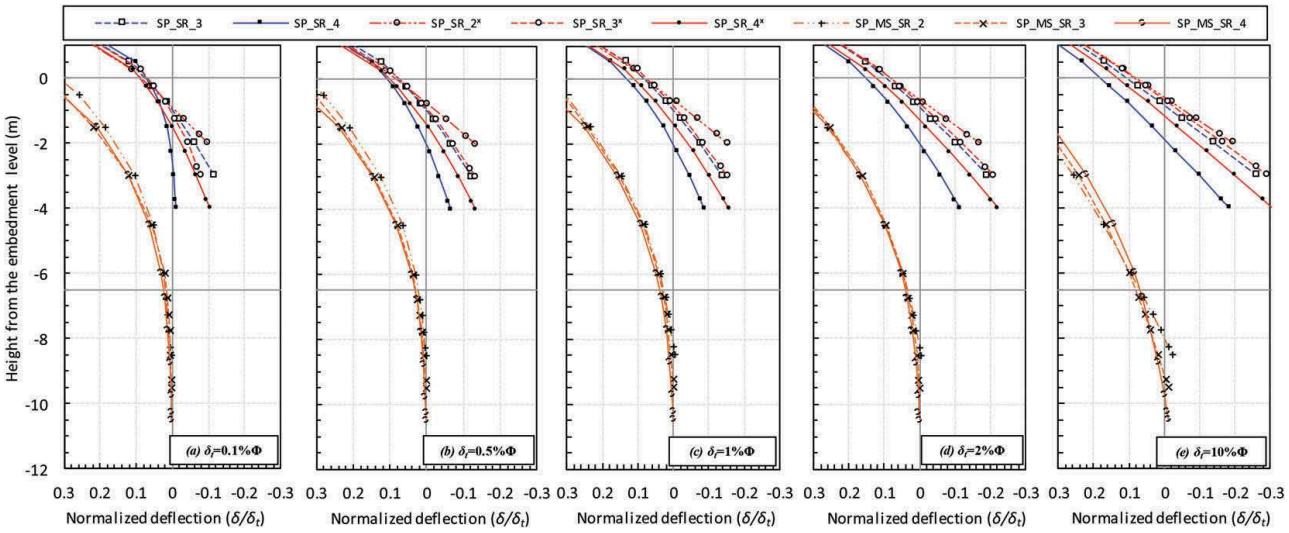


Figure 10. Estimated normalized deflection profiles at different imposed displacement amplitudes.

0.6 m (0.3Φ) below the rock surface as seen in Figure 10(c-e). Thanks to the large lateral confinement of rock type materials even at shallow depths, a small increment of socket depth $\Delta(d_R/\Phi)$ = 0.5, from $d_R/\Phi$ =1.0 and $d_R/\Phi$ =1.5 significantly increased the redundancy against the brittle softening and changed the deformation and failure mechanism from brittle to the ductile one.

The above can be confirmed from Figure 8(c,d) and Figure 10, while comparing the displacements and rotations at RS, BT for the piles SP_SR_3, SP_SR_3ˣ, SP_SR_4, SP_SR_4ˣ with those of pile SP_SR_2ˣ. Although the piles with $d_R/\Phi$ =1.5 (SP_SR_3 and SP_SR_3ˣ) exhibit a clear post-peak softening due to the rock failure and comparatively large displacements at BT level than that of RS (Figure 8(c)), significant redundancy against the ultimate collapse exists even in the post-peak response. It can be confirmed from the difference between RS and BT rotations of pile SP_SR_3ˣ and the pile SP_SR_3 even beyond the peak resistance as illustrated in Figure 8(d) and the bending fractions of piles even at a large imposed displacement of $\delta_t/\Phi$ =6, in Figure 9(a). Furthermore, the observed large residual resistances of more than 80% of $M_{L\_ult}$ in Figure 8(c,d) also another evidence of redundancy against brittle failures. As the $d_R/\Phi$ increases from 1.5 to 2, the ultimate failure mode has changed from ground failure to the structural buckling (SP_SR_4) as seen in Figure 5(a-2). The observed bending profile (Figure 7(f)), displacements and rotations at RS and BT, even at a large moment load (SP_SR_4) as illustrated in Figure 8(c,d) and the decrease of rotational and increase of bending fractions in Figure 9(a) also support this physical observation. The above observations of piles with $d_R/\Phi$ =1,1.5 and 2 indicates the change of load transfer mechanism, i.e., as $d_R/\Phi$ increases from 1.5 to 2, the depth-dependent bearing factors provides large rotational resistance due to high confinement at deep locations. It allows more strains in the pile front shallow rock layers (Figure 10) and causing significant deterioration of soft rock modulus. As a consequence, the deformation at the pile front rock surface is higher for the pile with $d_R$=4 m (SP_SR_4, SP_SR_4x) than $d_R$ =3 m (SP_SR_3, SP_SR_3x) under same imposed displacement as seen in Figure 10.

From Figure 9(b), all three piles MS_SR ground exhibit almost same displacements and rotations at SS and RS up to $\delta_t/\Phi$ =2% ($M_L$ =4 MNm) regardless of the rock socket depths. The observation indicates that, socketing over $d_R$ = $\Phi$ has no significant influence on the lateral and rotational resistances up to $\delta_t$ =2%$\Phi$. The above observation could be attributed to large lateral confinement and rotational resistance of intact rock sockets (initial subgrade modulus or smaller relative stiffness ($E_e/G^*$)), which mainly controls the pile deformation at the early stages of loading. However, the deviations beyond $\delta_t$ =2%$\Phi$ in Figure 9 (b) could be attributed to the increase in $E_e/G^*$ due to the deterioration in the subgrade modulus of soft rock. It can be confirmed from the increasing trend of rotation and decreasing trend of bending fractions of SS displacement as shown in Figure 9(c) and the normalized deflection profiles given in Figure 10. Furthermore, Figure 11(a) summarizes the influence of $d_R/\Phi$ on the % fractions of SS displacement. The deformation mechanism of piles below the SS is dominated by the bending fractions in the overlain sand layer up to certain % of $\delta_t$ at which the rotational fraction overcomes the bending as observed in Figure 9(c). This $\delta_t$ is about 2%, 4% and 8%$\Phi$ for the piles with $d_R/\Phi$ =1,1.5 and 2, respectively. These values of $\delta_t$ tends to increase with $d_R$ and exhibit significant recovery of rotations and increase of bending fractions as $d_R./\Phi$ increases in Figure 11(a). Based on above observations, at relatively small $\delta_t$ (< 2%$\Phi$) the displacement at overlain SS is dominated by the pile bending in the sand layer due to large lateral

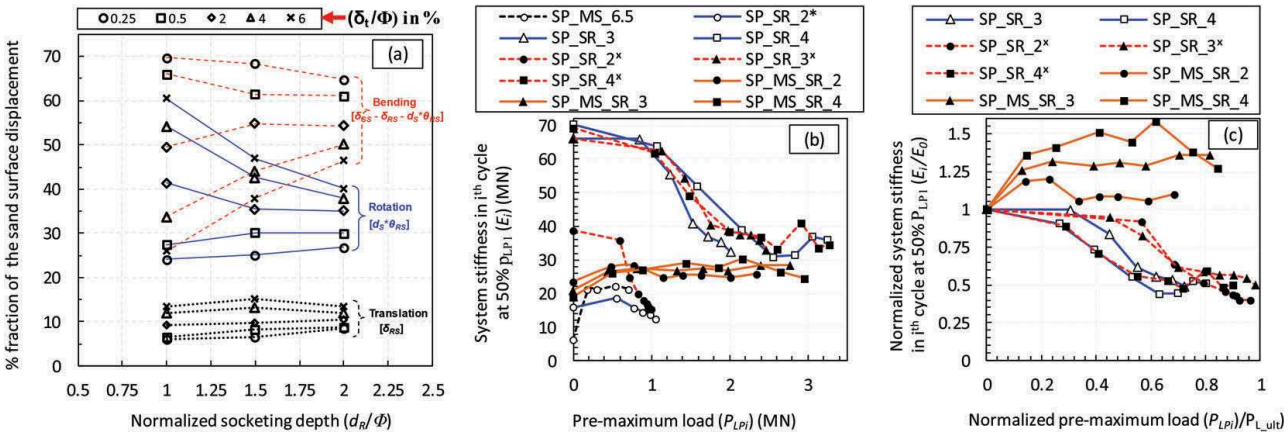


Figure 11. Influence of rock socketing depth on the lateral resistances of the piles single rock layer and two layer profile.

confinement of intact rock sockets. However, as $E_e/G^*$ of the system increases due to the deterioration of soft rock modulus, the displacement caused by the rotation at RS tends to dominate the bending fraction at SS. This ratio between rotation and bending fraction at a $\delta_t$ of 10% $\Phi$ tend to shrink from 4.5 to a value of unity as the $d_R$ increases from $d_R/\Phi$ =1 to 2.

### 3.5 *Change of system stiffness*

To investigate the embedment ground, structure conditions and the consequences of cyclic loading on the deterioration of ground stiffness, an initial system stiffness ($E_i$) is defined at 50%$P_{LP1}$ as described in Figure 2. The variation of $E_i$ values against $P_{LPi}$ and $P_{LPi}/P_{L\_ult}$ are plotted in Figure 11(b) and 11(c), respectively. From Figure 11(b), the differences of $E_0$ values between rock socketed piles with and without the overlain media can be confirmed. Except for the short socketed piles (SP_SR_2* and SP_SR_2×), the $E_0$ of piles directly socketed in the soft rock (SR) is about 2.5 and 3 times higher than those of embedded in MS_SR ground, at 50% $P_{LP1}$. The observation implies that the $E_0$ values highly depends on the stiffness of embedded ground rather than the embedment depth. Comparing the pile SP_SR_2× with SP_SR_3 and SP_SR_3× in Figure 11(b), the $E_0$ values could be increased about 50% by the increment of rock socketing $\Delta(d_R/\Phi)$ = 0.5 from $d_R/\Phi$ = 1.0. Meanwhile, a further increment from $d_R/\Phi$ = 1.5 (SP_SR_3 and SP_SR_3×) to 2 (SP_SR_4 and SP_SR_4×) has no remarkable contribution on the $E_0$ values of rock socketed pile as seen in Figure 11(b). Still, the deterioration of the system stiffness gradually occurred for those with a socket depth of $d_R/\Phi$ = 2 compared to those with $d_R/\Phi$ = 1.5 and the observation is more perceptible from Figure 11(b) than the normalised profiles illustrated in Figure 11 (c), showing the better redundancy for the former socket depth than the latter.

Similarly, in MS_SR ground, a 2 m ($d_R/\Phi$ = 1.0) rock socketing in the underlain rock layer has increased the $E_0$ values by about 4 times compared to the pile with zero socketing (SP_MS_6.5), it can be confirmed from the comparison of pile SP_MS_6.5 with the pile SP_MS_SR_2 in Figure 11 (b). Furthermore, a clear contribution of additional socketing also visible in the normalised relations illustrated in Figure 11(c), where $E_i/E_0$ increases with the increase of socket depth even at relatively large $P_{LPi}$ values (up to 60% $P_{L\_ult}$). The observed constant trend of $E_i$'s even at large $P_{LPi}$ values is a clear indication of system redundancy against the softening of underlain rock layer. It is also true from the ultimate failure mode as structural buckling for all three piles shown in Figure 5. Unlike the piles in MS_SR ground, for the piles in SR ground, the $E_i$ values steadily decreased from the second loading cycle, which indicates the softening in the stress-strain behaviour of soft rock and significant deterioration of the subgrade modulus or the foundation stiffness.

## 4 CONCLUSIONS

In the stiff ground like the soft rock, the lateral resistance changes significantly in a small range of embedment depth. A small increment of embedment depth (0.5Φ to 1Φ) in soft sand rock remarkably increased the redundancy against the brittle softening and changed the deformation mechanism from brittle to the ductile one.

The ultimate failure mechanism of rock socketed piles in a single rock layer is mainly caused by the rotation at RS when the ultimate resistance is determined by the rock failure. However, when the structural buckling determines the ultimate resistance, the mechanism is a combination of rotation at RS, translation at RS and the bending above the RS with the domination of rotational fraction.

In the two-layer profile; displacement at SS is dominated by the pile bending in the sand layer from the initiation of loading to a critical $\delta_t/\Phi$, over which the rotational fraction tends to dominate the bending. This critical $\delta_t/\Phi$ increases with the increase of $d_R$,

meanwhile at large imposed displacements or ultimate loads, the ratio between rotation and bending fractions tend to shrink from a value of 4.5 to unity as the rock socket depth increases from $d_R/\Phi$ =1 to 2.

## ACKNOWLEDGEMENT

The authors gratefully acknowledge the invaluable advice and guidance provided by the members and advisers of the IPA TC1 (Committee on Application of Cantilever Type Steel Tubular Pile Wall Embedded to Stiff Ground) in connection with the preparation of this paper.

## REFERENCES

Digioia AM, Rojas-Gonzalez LF (1994) Rock socket transmission line foundation performance. *IEEE transactions on power delivery* 9(3):1570–1576.

IPA (International Press-in Association) (2016) *Press-in Retaining Structure: A Handbook*, 1st ed.

Kunasegaram V, Akazawa S, Takemura J, Seki S, Fujiwara K, Ishihama Y, and Fujii Y,(2015) "Modeling of soft rock for a centrifuge study", *Proc. 12th Geo-Kanto*, pp. 15–19.

Kunasegaram V, Hsiao W.H, and Takemura J,(2018) "Behavior of a large diameter piles subjected to moment and lateral loads", *Proceedings of the 1st ICPE*, Kochi.

Kunasegaram V, Takemura J (2020) Deflection and failure of high-stiffness cantilever retaining wall embedded in soft rock. *IJPMG*: 1–21.

Kunasegaram V, Takemura J (2021). Mechanical behaviour of laterally loaded large-diameter steel tubular piles embedded in soft rock. *Geotechnical & Geological Engineering*, (*under review*).

Lehane BM, Guo F (2017) Lateral response of piles in cemented sand. *Géotechnique* 67(7):597–607.

Tatsuoka F, Goto S, Sakamoto M (1986) Effects of some factors on strength and deformation characteristics of sand at low pressures. *Soils and foundations* 26(1):105–114.